

AdarGCN: Adaptive Aggregation GCN for Few-Shot Learning

Jianhong Zhang¹, Manli Zhang¹, Zhiwu Lu^{*}, Tao Xiang², and Jirong Wen¹

¹Beijing Key Laboratory of Big Data Management and Analysis Methods
School of Information, Renmin University of China, Beijing 100872, China

²Department of Electrical and Electronic Engineering,
University of Surrey, Guildford, Surrey GU2 7XH, United Kingdom

Abstract

Existing few-shot learning (FSL) methods assume that there exist sufficient training samples from source classes for knowledge transfer to target classes with few training samples. However, this assumption is often invalid, especially when it comes to fine-grained recognition. In this work, we define a new FSL setting termed few-shot few-shot learning (FSFSL), under which both the source and target classes have limited training samples. To overcome the source class data scarcity problem, a natural option is to crawl images from the web with class names as search keywords. However, the crawled images are inevitably corrupted by large amount of noise (irrelevant images) and thus may harm the performance. To address this problem, we propose a graph convolutional network (GCN)-based label denoising (LDN) method to remove the irrelevant images. Further, with the cleaned web images as well as the original clean training images, we propose a GCN-based FSL method. For both the LDN and FSL tasks, a novel adaptive aggregation GCN (AdarGCN) model is proposed, which differs from existing GCN models in that adaptive aggregation is performed based on a multi-head multi-level aggregation module. With AdarGCN, how much and how far information carried by each graph node is propagated in the graph structure can be determined automatically, therefore alleviating the effects of both noisy and outlying training samples. Extensive experiments show the superior performance of our AdarGCN under both the new FSFSL and the conventional FSL settings.

1. Introduction

Few-shot learning (FSL) [18, 5] becomes topical. It aims to recognize a set of target classes by learning with suf-

*Corresponding author.

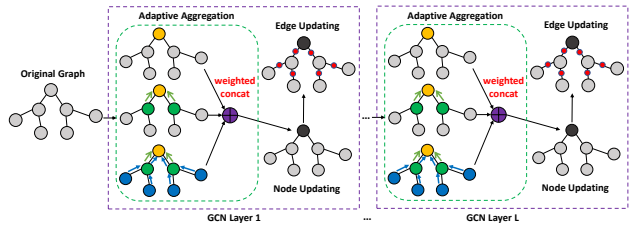


Figure 1. Illustration of our adaptive aggregation module.

ficient labelled samples from a set of source classes and only few labelled samples from the target classes. Existing FSL methods [25, 29, 6, 39, 41, 40, 1, 26] employ a deep neural network (DNN) model [15, 44, 10] as the backbone for FSL. They thus make the implicit assumption that there are sufficient training samples from the source classes for knowledge transfer to the target. However, this assumption is often invalid in practice especially when it comes to fine-grained recognition. For this problem, the source classes are also fine-grained, so collecting and labeling sufficient samples for each source class is also difficult. For example, in the widely-used CUB dataset [42], each bird class has less than 60 samples. Without sufficient labelled samples from source classes, it becomes harder to recognize the target classes by knowledge transfer from source classes.

In this work, we define a new setting termed few-shot few-shot learning (FSFSL), where only few labelled samples from both source and target classes are available for model training. To overcome the source class data scarcity problem under the FSFSL setting, a natural solution would be to crawl sufficient images from the web by searching with the name of each source class (e.g. utilizing Google Image Search). However, although the crawled data contain additional training images, it also inevitably consists of large quantities of irrelevant ones. To fully exploit the crawled noisy images of each source class for FSFSL, label denoising (LDN) is required as a preprocessing step.

Inspired by the successful use of graph convolutional

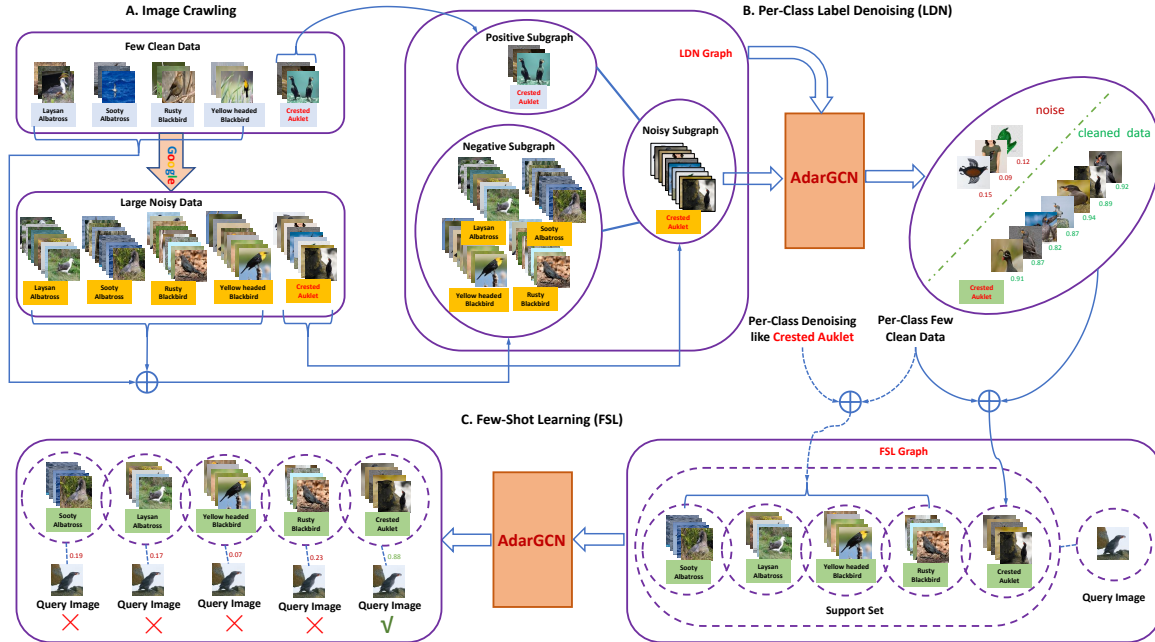


Figure 2. Schematic of the proposed AdarGCN model for few-shot few-shot learning (FSFSL).

network (GCN) [14, 4, 38, 7] in many vision problems, we focus on GCN-based LDN in this work. Specifically, for each source class, the few clean training images of this source class are used as the positive samples, while the clean and crawled images of the other source classes are used as the negative samples. Given a specific source class, although the crawled images of the other source classes are noisy, it is safe to assume that most if not all of them are negative w.r.t. this source class. This fact is taken advantage of when we design our GCN-based LDN model.

With the web images cleaned by our GCN-based LDN model, they can be merged with the original clean training images to form an enlarged training set. Our new FSFSL setting thus becomes the conventional one, and any existing FSL methods can be employed here. However, there are still noisy training images undetected by the LDN – no matter how effective it is, it is not perfect. Consequently, the FSL model must be able to cope with this data noise problem. To this end, we propose a novel GCN-based FSL method to better solve the FSL problem with the augmented noisy training data. Different from previous GCN-based FSL methods [33, 12, 8], we design an adaptive aggregation GCN (AdarGCN) which can perform adaptive aggregation based on a multi-head multi-level aggregation module (see Fig. 1). With our AdarGCN, how much and how far the information carried by each node is propagated to the rest of the graph structure is controlled by each head, making the propagation controllable and adaptive to each instance. An aggregation gate with learnable parameters is then used to dynamically determine the weight of each head when fusing multiple heads. In this way, the nega-

tive impact of a noisy training sample can be limited to a small neighborhood of the corresponding node, thus effectively diminishing its detrimental effect. As illustrated in Fig. 2, our AdarGCN is used to solve both tasks (i.e. LDN and FSL) because in both tasks, dealing with noisy training images is the key and our AdarGCN is effective under both the new and conventional FSL settings. We also empirically observe that with AdarGCN, (1) the GCN can be deeper than existing ones which are typically limited by the depth of layers due to over-smoothing, bringing additional performance gain, and (2) it beats the state-of-the-art alternatives even under the conventional FSL setting, indicating that AdarGCN benefits from dealing with the clean but outlying samples under the conventional FSL.

Our contributions are: (1) We define a new FSL setting termed FSFSL, which is more challenging yet more realistic than the conventional FSL setting. (2) A two-stage solution is provided for FSFSL: 1) crawling sufficient source class training images from the web and performing label denoising on them; 2) solving the FSL problem after merging the cleaned web images with the original training samples. (3) Both the LDN and FSL tasks involved in our FSFSL setting are addressed by proposing a novel GCN model termed AdarGCN. It is different from existing GCN models in that it can perform adaptive aggregation to alleviate the effects of noisy training samples. Extensive experiments show that our AdarGCN achieves state-of-the-art results under both FSL settings. The code and dataset will be released soon.

2. Related Work

Few-Shot Learning. Meta-learning based methods [25, 29, 6, 39, 41, 40, 24, 1, 16, 32] have dominated recent FSL research. Apart from metric learning solutions [39, 41, 40, 1], another promising approach is learning to optimize [29, 6, 16, 32]. More recently, methods based on feature hallucination and synthesis [9, 36] or predicting parameters of the network [28, 27] have been developed. However, the promising performance of existing FSL methods is highly dependent on the assumption that there exist sufficient training labelled samples. In this work, we thus focus on a new FSFSL setting (only with a few labelled samples per source class). Even though our AdarGCN is designed for this new setting, it is found to be extremely competitive under the conventional FSL setting (see Table 5). This suggests that the outlying samples problem, largely ignored by existing FSL methods so far, should also be addressed even if the source class data are plenty.

Graph Convolutional Networks. GCN is designed to work directly on graphs and leverage their structural information [14, 4, 38, 7]. Recently, GCN has been employed in various problems [46, 45, 37, 23, 43, 34, 17, 20, 21, 47]. In particular, label denoising with GCN [11, 8] has attracted much attention. In [11], its focus is on fully exploiting sufficient noisily labelled samples from target classes for FSL (which is against the standard FSL setting), and the core transfer problem implied in FSL remains unexplored. To overcome these drawbacks, we choose to study a new FSFSL setting in our current work. In [8], a GCN-based denoising autoencoder is proposed to generate the classification weights for both source and target classes under generalized FSL [35], but no GCN-based label denoising problem is concerned in [8]. Moreover, although GCN has been directly used in a number of recent FSL methods [33, 12, 8, 11], our AdarGCN is different in that it can perform adaptive aggregation for FSL and is able to cope with both noisy and outlying training samples. Our results show that the new GCN is clearly better (see Table 5).

3. Methodology

3.1. Problem Definition

We formally define the few-shot few-shot learning (FSFSL) problem as follows. Let C_s denote a set of source classes and C_t denote a set of target classes ($C_s \cap C_t = \emptyset$). We are given a k_1 -shot sample set \mathcal{D}_s from the source classes, a k -shot sample set \mathcal{D}_t from the target classes, and a test set \mathcal{T} from the target classes. Concretely, the first small sample set can be defined as $\mathcal{D}_s = \{(x_i, y_i) | y_i \in C_s, i = 1, \dots, N_s\}$, where y_i denotes the class label of sample x_i and N_s denotes the number of samples in \mathcal{D}_s . Since each source class from \mathcal{D}_s has only k_1 labelled samples, we have $N_s = k_1 |C_s|$. Similarly, the second small sample set

can be defined as $\mathcal{D}_t = \{(x_i, y_i) | y_i \in C_t, i = 1, \dots, N_t\}$, where $N_t = k |C_t|$ (each target class has k labelled samples). The goal of FSFSL is thus to train a model with \mathcal{D}_s that can generalize well to \mathcal{T} . Note that our new FSFSL problem is clearly more challenging than the conventional FSL problem, since \mathcal{D}_s only has few samples per class.

As in previous works [6, 39, 41, 40, 24], we train a FSL model with n -way k -shot classification tasks. Concretely, each n -way k -shot task is defined over a randomly-sampled episode $\{\mathcal{S}_e, \mathcal{Q}_e\}$, where \mathcal{S}_e is the support set having n classes and k samples per class, and \mathcal{Q}_e is the query set. Each episode is sampled as follows: we first sample a small set of source classes $C_e = \{C_i | i = 1, \dots, n\}$ from C_s , and then generate \mathcal{S}_e and \mathcal{Q}_e by sampling k support samples and q query samples from each class in C_e , respectively. Formally, we have $\mathcal{S}_e = \{(x_i, y_i) | y_i \in C_e, i = 1, \dots, n \times k\}$ and $\mathcal{Q}_e = \{(x_i, y_i) | y_i \in C_e, i = 1, \dots, n \times q\}$, where $\mathcal{S}_e \cap \mathcal{Q}_e = \emptyset$. A FSL model is then trained by minimizing the gap between its predicted labels and the ground-truth labels over the query set \mathcal{Q}_e .

3.2. Two-Stage Solution

To overcome the lack of training samples from source classes in FSFSL, we provide a two-stage solution, as shown in Figure 2. The first stage consists of image crawling and GCN-based LDN, as shown in Figure 2(A) and Figure 2(B). For each source class $c \in C_s$, we only have a small set of k_1 clean images initially: $X_c^s = \{x_i | (x_i, y_i) \in \mathcal{D}_s, y_i = c, i = 1, \dots, N_s\}$. To augment the small set X_c^s , we then crawl another set of k_2 additional images from the web by image searching with the name of source class $c \in C_s$: $X_c^{web} = \{x_i | i = 1, \dots, k_2\}$. As expected, there exists much noise in X_c^{web} . Therefore, we propose a GCN-based LDN method to reduce the noise in X_c^{web} and obtain a set of cleaned images $X_c^d \subset X_c^{web}$. We then define the set of denoised samples as: $\mathcal{D}_d = \{(x, y) | x \in X_c^d, y = c, c = 1, \dots, |C_s|\}$. Moreover, the second stage consists of GCN-based FSL, as shown in Figure 2(C). We leverage both \mathcal{D}_s and \mathcal{D}_d to train our GCN-based FSL model. For both the LDN and FSL tasks, we design an adaptive aggregation GCN (AdarGCN) model (see Figure 3).

3.3. GCN-Based LDN

In the first stage, we perform GCN-based LDN over the noisy images crawled for each source class. Specifically, given a source class $c \in C_s$, we have a positive image set $X_c^+ = X_c^s$, a noisy image set $X_c^* = X_c^{web}$, and a negative image set $X_c^- = \{X_i^+ \cup X_i^* | i \in C_s, i \neq c\}$, as shown in Fig. 2(B). Before per-class LDN, we pretrain a simple embedding network (e.g. four-block ConvNet) on X_c^+ like ProtoNet [39] to extract d -dimensional image feature vectors, which is consistent with the second stage (the same simple backbone is used for GCN-based FSL).

To construct an LDN graph for each source class $c \in C_s$, we generate a mini-batch by randomly selecting m^+ images from X_c^+ , m^* images from X_c^* , and m^- images from X_c^- (see Fig. 2(B)). The image feature matrices of these three groups of samples are respectively denoted as $V_c^+ \in \mathbb{R}^{m^+ \times d}$, $V_c^* \in \mathbb{R}^{m^* \times d}$, and $V_c^- \in \mathbb{R}^{m^- \times d}$. The node feature matrix is thus defined as $V_c = [V_c^+; V_c^*; V_c^-] = [v_1; \dots; v_M] \in \mathbb{R}^{M \times d}$, where $M = m^+ + m^* + m^-$. The initial symmetric adjacency matrix $A_c = \{a_{ij}\} \in \mathbb{R}^{M \times M}$ is defined as: $a_{ij} = 0$ if v_i and v_j respectively come from V_c^+ and V_c^- , and $a_{ij} = 1$ otherwise (see Fig. 2(B)). This choice of constructing A_c ensures that the positive and negative samples cannot be directly confused by each other.

We denote the above LDN graph as $\mathcal{G}_c = (V_c, E_c)$, where the edge feature matrix $E_c = \{e_{ij}\} \in \mathbb{R}^{M \times M}$. In this work, we exploit a 3-layer AdarGCN model for label denoising, which is defined in Section 3.5. Specifically, to adapt AdarGCN to the LDN task, we make four modifications to its architecture: (1) For each edge updating (EU) unit, we set $e_{ij} = 0$ when $a_{ij} = 0$, after the sigmoid operation to avoid direct label confusion during label propagation. (2) Before the node updating (NU) unit of the first GCN layer, we perform EU to initialize E_c . (3) For each NU unit, we perform a linear transformation after the concat operation. (4) For the last GCN layer, we drop the EU unit and use a sigmoid function to output the predicted score for each sample.

Note that our GCN-based LDN model can be regarded as a binary classifier, outputting 1 for positive samples and 0 for negative ones. However, unlike the traditional image classification, our model can make full use of uncertain samples (i.e. images from X_c^*) by aggregating similar nodes for more effective label propagation. Let \hat{y}_i be the predicted score of each sample x_i ($i = 1, \dots, M$). The loss for GCN-based LDN is defined as follows:

$$\mathcal{L}_{LDN} = -\frac{1}{m^+} \sum_{i=1}^{m^+} \log(\hat{y}_i) - \frac{1}{m^-} \sum_{i=M-m^-+1}^M \log(1 - \hat{y}_i). \quad (1)$$

Although our GCN-based LDN model ignores the direct back-propagation w.r.t. the loss of noisy images (whose labels are uncertain), it can learn better representation for uncertain images by aggregating both certain and uncertain images, followed by back-propagation w.r.t. the loss of certain images. Notably, our GCN-based LDN model is shown to outperform multi-layer perceptron (MLP) which copes with each sample independently (see Table ??).

After the GCN training process, since each uncertain sample $x \in X_c^*$ appears in multiple LDN graphs w.r.t. source class c , we average the obtained multiple predicted scores as the probability of being positive for each sample x . If this probability is greater than a preset threshold, we then add (x, c) to the set of denoised samples \mathcal{D}_d .

3.4. GCN-Based FSL

In the second stage, given $\mathcal{D}_s \cup \mathcal{D}_d$, we train our GCN-based FSL model by episodic sampling. For each episode, we randomly select $n \times k$ samples to form the support set \mathcal{S}_e and $n \times q$ samples to form the query set \mathcal{Q}_e . The embedding network f_φ is trained jointly with the GCN module to obtain the feature representations of all samples from $\mathcal{S}_e \cup \mathcal{Q}_e$: $v_i = f_\varphi(x_i)$, $i = 1, \dots, n \times (k+q)$. Although both transductive (with all query images in one trial) and non-transductive (with a single query image per trial) test strategies are followed in [12], we only adopt the non-transductive strategy for fair comparison, since most of the state-of-the-art FSL methods are non-transductive. Concretely, for each episode, we construct $n \times q$ graphs, each of which is defined over $n \times k$ support samples and 1 query sample.

We collect the above $n \times q$ graphs as $\mathcal{G} = \{\mathcal{G}_t = (V_t, E_t) | t = 1, \dots, n \times q\}$. For a single graph \mathcal{G}_t in \mathcal{G} ,

$V_t = \{\overbrace{v_1^s, \dots, v_{n \times k}^s}^{\mathcal{S}_e}, \overbrace{v_t^q}^{\mathcal{Q}_e}\}$. Concisely, we take it as $V_t = \{v_i\}_{i=1}^{n \times k+1}$, along with $E_t = \{e_{ij}\}_{i,j=1, \dots, n \times k+1}$, where v_i is the node feature obtained by the embedding network, $v_{n \times k+1}$ denotes the node feature of the query image, and e_{ij} is the edge feature w.r.t. v_i and v_j . For $v_i, v_j \in \mathcal{S}_e$, $e_{ij} = 1$ if v_i and v_j come from the same class and $e_{ij} = 0$ otherwise. When $v_i \notin \mathcal{S}_e$ or $v_j \notin \mathcal{S}_e$, we also set $e_{ij} = 0$ due to the unknown label of v_i or v_j .

The full GCN-based FSL model is stacked by L GCN layers with the same AdarGCN architecture shown in Figure 3. In this work, we set $L = 3$. Given a graph \mathcal{G}_t ($t = 1, \dots, n \times q$), the inputs of the first GCN layer (i.e. node feature matrix V_t^0 and edge feature matrix E_t^0) are obtained in the way mentioned above (where we set $l = 0$). For the l -th GCN layer ($l = 1, \dots, L$), the inputs V_t^{l-1} and E_t^{l-1} (from the previous layer) are updated to V_t^l and E_t^l .

For GCN training, we choose the binary cross-entropy loss between the ground-truth edge matrix $E^{gt} = \{e_{ij}^{gt}\}_{i,j=1, \dots, n \times k+1}$ and the edge feature matrices of all L GCN layers $\{E_t^l = \{e_{ij}^l\}_{i,j=1, \dots, n \times k+1}\}_{l=1}^L$, where $e_{ij}^{gt} = 1$ if x_i and x_j come from the same class and $e_{ij}^{gt} = 0$ otherwise. Formally, for each graph \mathcal{G}_t , the binary cross-entropy loss of the l -th GCN layer is defined as:

$$\mathcal{L}_t^l = -\sum_{i=1}^{n \times k+1} \sum_{j \neq i} e_{ij}^{gt} \cdot \log(e_{ij}^l) + (1 - e_{ij}^{gt}) \cdot \log(1 - e_{ij}^l). \quad (2)$$

Taking all graphs (each for a query image) and all GCN layers on board, we compute the overall cross-entropy loss for a training episode as follows:

$$\mathcal{L}_{FSL} = \sum_{t=1}^{n \times q} \sum_{l=1}^L \lambda^l \cdot \mathcal{L}_t^l, \quad (3)$$

where λ^l denotes the loss weight of the l -th GCN layer.

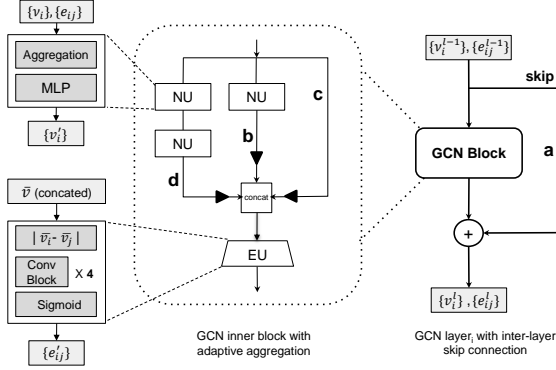


Figure 3. Illustration of the network architecture of our AdarGCN model. Notations: NU – node updating; EU – edge updating.

For GCN inference, the edge feature matrix E_t^L of the last GCN layer can be used to predict the label of the unique query image. Concretely, the predicted scores of the query image are collected as $\hat{y} = \{\hat{y}_1, \dots, \hat{y}_{n \times k}\}$, where $\hat{y}_i = e_{n \times k + 1, i}^L$ ($0 \leq \hat{y}_i \leq 1$), being the predicted probability of the query image coming from the class that support sample x_i belongs to ($i = 1, \dots, n \times k$). The classification probability of the query image is:

$$p_c = \sum_{i=1}^{n \times k} \mathbb{1}(y_i = c) \cdot \hat{y}_i / \sum_{i=1}^{n \times k} \hat{y}_i, \quad (4)$$

where $\mathbb{1}$ denotes the indicator function, y_i denotes the class label of support sample x_i , and c denotes the c -th class label in the episode ($c = 1, \dots, n$).

3.5. Network Architecture of AdarGCN

For both LDN and FSL tasks involved in our FSFSL setting, we design an AdarGCN model, as illustrated in Figure 3. Different from existing GCN models [33, 12, 8, 14, 19]), our AdarGCN induces adaptive aggregation into GCN training to better control the information propagation from each node to the rest to the graph structure.

Formally, for the l -th GCN layer ($l = 1, \dots, L$) of our AdarGCN, given the node feature matrix V^{l-1} and the edge feature matrix E^{l-1} as inputs, the output V^l can be obtained by adding the node feature matrix from the GCN inner block and that from the previous GCN layer:

$$V^l = V^{l-1} + V_{block}, \quad (5)$$

which is essentially implemented by the inter-layer skip-connection branch **a** (see Figure 3).

Within the GCN inner block of the l -th GCN layer, we design a multi-head multi-level aggregation module to aggregate the node features adaptively with different aggregation complexities, as illustrated in Figure 3. For this GCN inner block, we choose to update the node feature matrix and edge feature matrix successively.

Specifically, node feature updating is achieved by the adaptive aggregation among the three updating branches **c**, **b**, **d** with different degrees of aggregation. Branches **c**, **b**, **d** update the node features respectively with 0, 1, 2 iterations: one iteration update is denoted by a Node Updating (NU) unit which consists of an aggregation module and a MLP module. The outputs of branches **c**, **b**, **d** are given by:

$$\begin{aligned} V_c^l &= V^{l-1}, \\ V_b^l &= f_{\theta_b}(E^{l-1} \cdot V^{l-1}), \\ V_d^l &= f_{\theta_{d1}}(E^{l-1} \cdot f_{\theta_{d2}}(E^{l-1} \cdot V^{l-1})), \end{aligned} \quad (6)$$

where θ_b collects the parameters of the MLP module in branch **b**, while θ_{d1} and θ_{d2} collect the parameters of the two MLP modules in branch **d**, respectively. As illustrated in Figure 1, how far information can travel along each head/branch differs – **d** has the farthest influence whilst **c** the shortest (each node itself). For adaptive aggregation, the adaptive weight of each of branches **c**, **b**, **d** is computed with a fully connected (FC) layer:

$$w_c = \text{FC}(V_c^l), \quad w_b = \text{FC}(V_b^l), \quad w_d = \text{FC}(V_d^l), \quad (7)$$

where $\text{FC}(\cdot)$ denotes the output of a FC layer, followed by a sigmoid function. The total node update within the GCN inner block is formulated as:

$$\bar{V}^l = \text{concat}(w_c \cdot V_c^l, w_b \cdot V_b^l, w_d \cdot V_d^l). \quad (8)$$

Note that more than three branches can be employed here, but empirically we found that more branches leads to no further gains. We thus use only three branches in this work.

For edge feature updating, we denote it with an Edge Updating (EU) unit. EU aims to learn the distance metric given node features as inputs, which includes a distance computing operation, 4 conv blocks, and a sigmoid activation function, as shown in Figure 3.

4. Experiments

4.1. New FSFSL

4.1.1 Datasets and Settings

Datasets. Two benchmark datasets are selected: (1) **mini-ImageNet**: This dataset is proposed in [41] and derived from ILSVRC-12 [31]. It consists of 100 classes totally. As in [29], this dataset is split into 64 training classes, 16 validation classes, and 20 test classes. Each image is resized to 84×84 . (2) **CUB**: The CUB dataset [42] is particularly suitable for our new FSFSL setting. Concretely, since the number of images per class is less than 60, the FSL problem on CUB is essentially a FSFSL problem. Although CUB has widely used for FSL, this work is the first to identify the problem and to provide a solution. This dataset consists

of 200 bird species totally. We split CUB into 100 training classes, 50 validation classes, and 50 test classes. Each image is also resized to 84×84 .

FSFSL Settings. Let k_1 be the number of original clean images per training class (i.e. source class), and k_2 be the number of crawled noisy images per training class. In this work, we set $k_1=10, 20$, or 50 , and $k_2=1,200$. As in the state-of-the-art works on GCN-based FSL [33, 12], the four-block ConvNet network is used as the embedding network. For both LDN and FSL tasks involved in our new FSFSL setting, the same embedding network is used. As in [33, 12], the 5-way 5-shot accuracy is computed over 600 episodes randomly sampled from the test set: each test episode have 5 support images and 15 query images per class. Although both transductive and non-transductive test strategies are followed in [12], we only take the non-transductive test strategy on board for fair comparison, since most of the state-of-the-art FSL methods are non-transductive.

Implementation Details. (1) **GCN-Based LDN:** The four-block ConvNet network pretrained on the training set is used as the feature extractor. The dimensionality of the output features is 128. For GCN training over each training class, a mini-batch consists of three types of images from this class: 5 positive images, 5 negative images, and 50 crawled noisy images¹ (see Figure 2). We construct an LDN graph over each mini-batch. We set a learning rate of 0.001, a dropout probability of 0.5, and a mini-batch size of 8. We adopt the Adam optimizer [13], with totally 500 training epochs. For each training class, we select the denoised images with prediction scores ≥ 0.5 for the subsequent GCN-based FSL task. (2) **GCN-Based FSL:** With the same 4-block embedding network, our GCN model for FSL is trained by the Adam optimizer [13] with a initial learning rate of 0.001 and a weight decay of $1e-6$. We also use label smoothing as in [16]. During the training phase, we cut the learning rate in half every 10,000 episodes and set total training episodes as 50,000. In the 5-way 5-shot scenario, each mini-batch has 32 training episodes, and each episode consists of 25 support images and 5 query images (5 shot support samples and 1 query sample per class). Within a training episode, we construct a graph over 25 support images and 1 query image for each query image.

Compared Methods. Since our FSFSL setting includes both LDN and FSL tasks, we compare our AdarGCN-LDN and AdarGCN-FSL with various LDN and FSL alternatives, respectively. When comparing our AdarGCN-LDN with other LDN methods including label propagation (LP) [48, 49], MLP, GCN [14] and ResGCN [19], we employ the same subsequent FSL model (i.e. AdarGCN-FSL) for fair comparison. Note that a score threshold of 0.5 is selected

¹Out of these crawled images, around 40% are noise. After LDN using our AdaGCN, this percent is reduced to around 10%. Some examples of the removed images can be found in the suppl. material.

Method	$k_1=10$	$k_1=20$	$k_1=50$
FSL (w/o crawled noisy images)	40.91	50.01	55.04
FSL (w/ crawled noisy images)	59.20	59.37	59.64
FSL+LDN (LP)	60.21	62.83	64.74
FSL+LDN (MLP)	60.19	62.88	64.25
FSL+LDN (GCN [14])	61.22	63.27	65.36
FSL+LDN (ResGCN [19])	61.48	63.79	65.92
FSL+LDN (ours)	63.37	65.12	66.85

Table 1. Comparative results by various label denoising (LDN) methods under the new FSFSL setting on mini-ImageNet. FSL denotes our GCN-based FSL method with our AdarGCN model.

Method	$k_1=10$	$k_1=20$	$k_1=50$
FSL (w/o crawled noisy images)	58.89	68.33	76.16
FSL (w/ crawled noisy images)	76.35	76.83	77.18
FSL+LDN (LP)	76.94	77.98	78.87
FSL+LDN (MLP)	77.10	78.06	78.92
FSL+LDN (GCN [14])	77.44	78.56	79.32
FSL+LDN (ResGCN [19])	77.52	78.69	79.69
FSL+LDN (ours)	79.16	79.82	80.88

Table 2. Comparative results by various label denoising (LDN) methods under the new FSFSL setting on CUB. FSL denotes GCN-based FSL with our AdarGCN model.

for all LDN methods except LP to classify the positive and negative samples. For LP-based LDN, a score threshold of 0 is used otherwise, since the positive samples are labelled as ‘1’ and the negative samples as ‘-1’. Similarly, when comparing our AdarGCN-FSL with various FSL baselines, we adopt the same LDN model (i.e. LDN-AdarGCN) for fair comparison. We focus on representative/state-of-the-art FSL methods including MatchingNet [41], MAML [6], ProtoNet [39], IMP [1], Baseline++ [3], GCN [33], wDAE-GNN [8], and EGCN [12].

4.1.2 Comparison to LDN Alternatives

The comparative results for the label denoising task on the two datasets are shown in Tables 1 and 2, respectively. It can be seen that: (1) Adding the crawled images (although noisy) to the original few clean training data leads to consistent and significant improvements for different values of k_1 . The improvements are particularly salient when k_1 takes a smaller value. (2) All LDN methods can further improve the FSL performance (see ‘FSL+LDN’ vs. ‘FSL (w/ crawled noisy images)’) by imposing label denoising over the crawled images, showing the effectiveness of LDN under our new FSFSL setting. (3) Our AdarGCN-LDN achieves the best label denoising results among all LDN methods. This suggests that GCN is suitable for label denoising, and adaptive aggregation included in our GCN model (i.e. AdarGCN) yields further improvements.

Method	mini-ImageNet	CUB
LDN+FSL (MatchingNet [41])	51.59	66.12
LDN+FSL (MAML [6])	59.67	73.50
LDN+FSL (ProtoNet [39])	64.73	74.48
LDN+FSL (IMP [1])	65.44	78.61
LDN+FSL (Baseline++ [3])	64.55	77.90
LDN+FSL (GCN [33])	64.80	74.59
LDN+FSL (wDAE-GNN [8])	63.26	74.23
LDN+FSL (EGCN [12])	65.12	78.10
LDN+FSL (ours)	66.85	80.88

Table 3. Comparative results by various FSL methods under the new FSFSL setting ($k_1=50$, $k_2=1,200$) on the two datasets. LDN denotes GCN-based LDN with our AdarGCN model.

GCN Model	LDN	FSL
AdarGCN (branch: b)	64.36	63.13
AdarGCN (branches: a, b)	65.92	65.01
AdarGCN (branches: a, b, c)	66.10	65.88
AdarGCN (branches: a, b, c, d)	66.85	66.85

Table 4. Ablative results for our AdarGCN model on both LDN and FSL tasks involved in our new FSFSL setting ($k_1=50$, $k_2=1,200$) over mini-ImageNet.

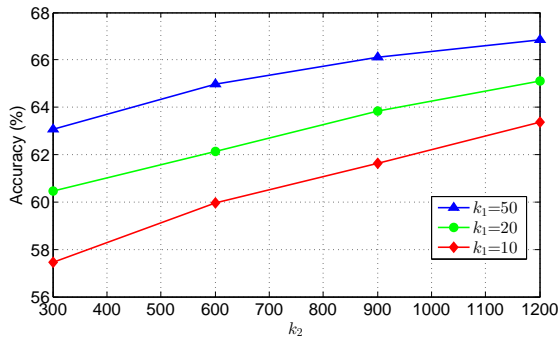


Figure 4. Illustration of the effect of different values of k_2 on our AdarGCN-LDN method over mini-ImageNet.

4.1.3 Comparison to FSL Alternatives

The comparative results for the FSL task on the two datasets are shown in Table 3. For fair comparison, all compared methods make use of the same set of denoised samples obtained by our AdarGCN-LDN method. We have the following observations: (1) Our AdarGCN-FSL method performs the best among all FSL methods, validating the effectiveness of our AdarGCN for solving the FSL task. (2) Our method clearly outperforms the latest GCN-based FSL methods [33, 12, 8], which suggests that adaptive aggregation indeed plays an important role when applying GCN to FSL. (3) Our method also clearly leads to improvements over the state-of-the-art FSL baselines [1, 3], showing that AdarGCN is a promising model to solve the FSL task.

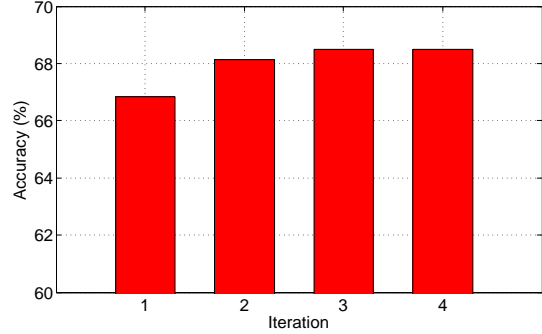


Figure 5. Illustration of the effect of iterative optimization on our AdarGCN-LDN method ($k_1=50$, $k_2=1,200$) over mini-ImageNet.

4.1.4 Further Evaluations

Ablation Study Results. The ablative results for our AdarGCN model on both the LDN and FSL tasks involved in our new FSFSL setting ($k_1=50$, $k_2=1,200$) are presented in Table 4. Note that AdarGCN-FSL is used for the ablation study on the LDN task, while AdarGCN-LDN is used for the ablation study on the FSL task. We can observe from Table 4 that adding more branches leads to more performance improvements on both the LDN and FSL tasks, consistently demonstrating the contribution of each branch (a, b, c, or d in Figure 3) in our AdarGCN model.

Effect of Different Values of k_2 . To show the effect of different values of k_2 on our AdarGCN-LDN method, we choose to gradually reduce k_2 from 1,200 to 300, and then evaluate the obtained LDN results by forwarding them to the subsequent FSL task (where our AdarGCN-FSL is used). The results in Figure 4 show that our AdarGCN-LDN method suffers from gradual performance degradation when k_2 decreases from 1,200 to 300. This is essentially consistent with the characteristic of image search engine (i.e. Google): when less relevant images are returned for each source class, there exist less images that truly belong to this source class, resulting in that less denoised training samples can be obtained for the subsequent FSL task (and thus performance degradation is caused).

Iterative Optimization for GCN-Based LDN. Note that the denoised samples obtained by our AdarGCN-LDN method can be easily exploited for another round of GCN-based LDN. In this work, for computational efficiency, we have ignored such iterative optimization in all of the above experiments. To show the effect of iterative optimization on our AdarGCN-LDN method, we present the results obtained by iterative optimization in Figure 5. We can observe that our AdarGCN-LDN method consistently achieves more improvements when more rounds of GCN-based LDN are included and becomes stable after three iterations.

Models	mini-ImageNet	CUB
MatchingNet [41]	55.30	68.71
ProtoNet [39]	65.77	74.70
Meta-Learn LSTM [29]	60.20	–
Reptile [25]	62.74	–
MAML [6]	63.11	71.33
Relation Net [40]	67.07	69.66
PPA [28]	67.87	–
TPN [22]	69.86	–
Shot-Free Meta [30]	65.73	–
R2-D2 [2]	68.40	–
IMP [1]	68.10	71.87
Baseline++ [3]	66.43	75.39 [†]
MetaOptNet [16]	69.51	77.10
GCN [33]	66.41	74.07
wDAE-GNN [8]	65.91	73.85
EGCN [12]	66.85	74.58
AdarGCN (ours)	71.48[‡]	78.04

Table 5. Comparative results under the conventional FSL setting. [†] denotes that the result is reproduced since our data split of CUB is different from that in [3]. [‡] note that our AdarGCN achieves an even higher accuracy of **72.24** with six GCN layers (see Figure 7).

4.2. Conventional FSL

4.2.1 Datasets and Settings

We further evaluate our AdarGCN-FSL method under the conventional FSL setting. The full mini-ImageNet and CUB datasets are selected for performance evaluation, where mini-ImageNet has 600 samples per class and CUB has less than 60 samples per class. The non-transductive 5-way 5-shot test strategy is adopted, exactly the same as the test strategy used for our new FSFSL setting. Moreover, the implementation details for GCN training remain largely unchanged compared to those described in Section 4.1.1. One exception is that: since the number of training samples in the CUB dataset is relatively small, we cut the learning rate in half every 5,000 episodes and set the total number of training episodes as 20,000 on CUB for better optimization.

4.2.2 Comparison to FSL Baselines

The following FSL baselines are selected: (1) State-of-the-art GCN-based FSL methods [33, 12, 8]; (2) Representative/latest FSL methods (w/o GCN) [39, 6, 40, 30, 2, 1, 3, 16]. The comparative results under conventional FSL are shown in Table 5. It can be seen that: (1) Our AdarGCN-FSL method yields 3–5% improvements over the latest GCN-based FSL methods [33, 12, 8], validating the effectiveness of adaptive aggregation for GCN-based FSL. (2) The improvements achieved by our method over the state-of-the-art FSL baselines [30, 2, 1, 3, 16] range from 1% to 6%, showing that AdarGCN has a great potential for FSL even with sufficient and clean training samples, due to its

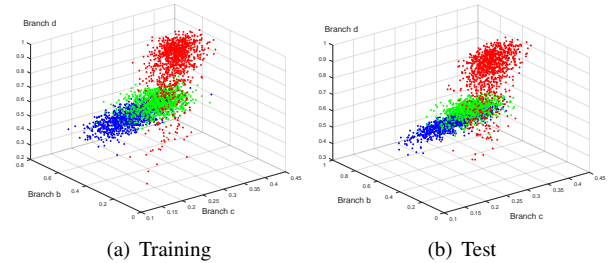


Figure 6. Illustration of weight distribution on the three branches **b**, **c**, **d** of different GCN layers obtained by our adaptive aggregation module over mini-ImageNet. The **red**, **green**, and **blue** points denote the weights of GCN layer **1**, **2**, and **3**, respectively.

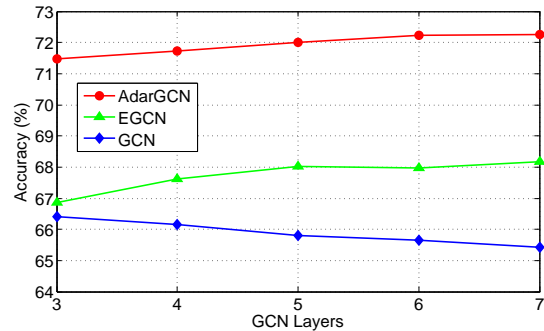


Figure 7. Comparative results among the three latest GCN-based FSL methods with deeper GCNs over mini-ImageNet.

ability to limit the negative effect of outlying samples.

4.2.3 Further Evaluations

Visualization of Adaptive Aggregation. By randomly sampling 1,000 query images respectively from the training set and the test set, we visualize the weights of the three branches **b**, **c**, **d** of different GCN layers obtained by our adaptive aggregation module (see Figure 3). The visualization results over mini-ImageNet are presented in Figure 6. It shows that each GCN layer has a significantly different weight distribution. This provides direct evidence that adaptive aggregation is indeed needed in GCN-based FSL. Further, it is also noted that the weight of branch **c** is forced to be significantly larger than those of the other two branches for the outlying samples so that their negative effect can be effectively limited (see the suppl. material).

FSL with Deeper GCN. In all above experiments, each GCN-based FSL method uniformly sets the number of GCN layers to 3, because it is well-known that deeper GCNs often lead to performance degradation. However, since both adaptive aggregation and skip connection are included in our AdarGCN model, it is possible to solve the FSL task with deeper AdarGCN. To explore the challenging problem of FSL with deeper GCNs, we provide the comparative results among the three latest GCN-based FSL methods (i.e. GCN [33], EGCN [12], and our AdarGCN) in Fig-

ure 7, where the number of GCN layers ranges from 3 to 7. As expected, the performance of GCN [33] drops when it goes deeper. However, both EGCN [12] and our AdarGCN achieve performance improvements when more GCN layers are stacked, and our AdarGCN consistently outperforms EGCN. This can be explained as: our AdarGCN leverages both adaptive aggregation and skip connection, while only skip connection is concerned in EGCN.

5. Conclusion

We have defined a new few-shot few-shot learning (FS-FSL) setting. To overcome the training source class data scarcity problem, we chose to augment the training data by crawling sufficient images from the web. Since the crawled images are noisy, we then proposed a GCN-based LDN method to clean the crawled noisy images. Further, with the cleaned web images and the original clean training images as the new training set, we proposed a GCN-based FSL method. For both the LDN and FSL tasks, we designed an AdarGCN model which can perform adaptive aggregation to deal with noisy training data. Extensive experiments demonstrate that our AdarGCN outperforms the state-of-the-art alternatives under both FSL settings.

References

- [1] Kelsey R. Allen, Evan Shelhamer, Hanul Shin, and Joshua B. Tenenbaum. Infinite mixture prototypes for few-shot learning. In *ICML*, pages 232–241, 2019. 1, 3, 6, 7, 8
- [2] Luca Bertinetto, Joao F Henriques, Philip HS Torr, and Andrea Vedaldi. Meta-learning with differentiable closed-form solvers. In *ICLR*, 2019. 8
- [3] Wei-Yu Chen, Yen-Cheng Liu, Zsolt Kira, Yu-Chiang Frank Wang, and Jia-Bin Huang. A closer look at few-shot classification. In *ICLR*, 2019. 6, 7, 8
- [4] Michaël Defferrard, Xavier Bresson, and Pierre Vandergheynst. Convolutional neural networks on graphs with fast localized spectral filtering. In *Advances in Neural Information Processing Systems*, pages 3844–3852, 2016. 2, 3
- [5] Li Fe-Fei, Rob Fergus, and Pietro Perona. A bayesian approach to unsupervised one-shot learning of object categories. In *ICCV*, pages 1134–1141, 2003. 1
- [6] Chelsea Finn, Pieter Abbeel, and Sergey Levine. Model-agnostic meta-learning for fast adaptation of deep networks. In *ICML*, pages 1126–1135, 2017. 1, 3, 6, 7, 8
- [7] Hongyang Gao, Zhengyang Wang, and Shuiwang Ji. Large-scale learnable graph convolutional networks. In *KDD*, pages 1416–1424, 2018. 2, 3
- [8] Spyros Gidaris and Nikos Komodakis. Generating classification weights with GNN denoising autoencoders for few-shot learning. In *CVPR*, pages 21–30, 2019. 2, 3, 5, 6, 7, 8
- [9] Bharath Hariharan and Ross Girshick. Low-shot visual recognition by shrinking and hallucinating features. In *ICCV*, pages 3037–3046, 2017. 3
- [10] Kaiming He, Xiangyu Zhang, Shaoqing Ren, and Jian Sun. Deep residual learning for image recognition. In *CVPR*, pages 770–778, 2016. 1
- [11] Ahmet Iscen, Giorgos Tolias, Yannis Avrithis, Ondrej Chum, and Cordelia Schmid. Graph convolutional networks for learning with few clean and many noisy labels. *arXiv preprint arXiv:1910.00324*, 2019. 3
- [12] Jongmin Kim, Taesup Kim, Sungwoong Kim, and Chang D. Yoo. Edge-labeling graph neural network for few-shot learning. In *CVPR*, pages 11–20, 2019. 2, 3, 4, 5, 6, 7, 8, 9
- [13] Diederik P. Kingma and Jimmy Ba. Adam: A method for stochastic optimization. In *ICLR*, 2015. 6
- [14] Thomas N Kipf and Max Welling. Semi-supervised classification with graph convolutional networks. *arXiv preprint arXiv:1609.02907*, 2016. 2, 3, 5, 6
- [15] Yann LeCun, Yoshua Bengio, and Geoffrey Hinton. Deep learning. *Nature*, 521(7553):436–444, 2015. 1
- [16] Kwonjoon Lee, Subhansu Maji, Avinash Ravichandran, and Stefano Soatto. Meta-learning with differentiable convex optimization. In *CVPR*, pages 10657–10665, 2019. 3, 6, 8
- [17] Ron Levie, Federico Monti, Xavier Bresson, and Michael M Bronstein. CayleyNets: Graph convolutional neural networks with complex rational spectral filters. *IEEE Transactions on Signal Processing*, 67(1):97–109, 2018. 3
- [18] Fei-Fei Li, Robert Fergus, and Pietro Perona. One-shot learning of object categories. *IEEE Transactions on Pattern Analysis and Machine Intelligence (TPAMI)*, 28(4):594–611, 2006. 1
- [19] Guohao Li, Matthias Müller, Ali Thabet, and Bernard Ghanem. Can GCNs go as deep as CNNs? In *ICCV*, 2019. 5, 6
- [20] Qimai Li, Zhichao Han, and Xiao-Ming Wu. Deeper insights into graph convolutional networks for semi-supervised learning. In *AAAI*, pages 3538–3545, 2018. 3
- [21] Zhuwen Li, Qifeng Chen, and Vladlen Koltun. Combinatorial optimization with graph convolutional networks and guided tree search. In *Advances in Neural Information Processing Systems*, pages 539–548, 2018. 3

- [22] Yanbin Liu, Juho Lee, Minseop Park, Saehoon Kim, Eunho Yang, Sung Ju Hwang, and Yi Yang. Learning to propagate labels: Transductive propagation network for few-shot learning. In *ICLR*, 2018. 8
- [23] Jianxin Ma, Peng Cui, Kun Kuang, Xin Wang, and Wenwu Zhu. Disentangled graph convolutional networks. In *ICML*, pages 4212–4221, 2019. 3
- [24] Nikhil Mishra, Mostafa Rohaninejad, Xi Chen, and Pieter Abbeel. A simple neural attentive meta-learner. In *ICLR*, 2018. 3
- [25] Alex Nichol, Joshua Achiam, and John Schulman. On first-order meta-learning algorithms. *arXiv preprint arXiv:1803.02999*, 2018. 1, 3, 8
- [26] Zhimao Peng, Zechao Li, Junge Zhang, Yan Li, Guo-Jun Qi, and Jinhui Tang. Few-shot image recognition with knowledge transfer. In *ICCV*, pages 441–449, 2019. 1
- [27] Hang Qi, Matthew Brown, and David G. Lowe. Low-shot learning with imprinted weights. In *CVPR*, pages 5822–5830, 2018. 3
- [28] Siyuan Qiao, Chenxi Liu, Wei Shen, and Alan L Yuille. Few-shot image recognition by predicting parameters from activations. In *CVPR*, pages 7229–7238, 2018. 3, 8
- [29] Sachin Ravi and Hugo Larochelle. Optimization as a model for few-shot learning. In *ICLR*, 2017. 1, 3, 5, 8
- [30] Avinash Ravichandran, Rahul Bhotika, and Stefano Soatto. Few-shot learning with embedded class models and shot-free meta training. In *ICCV*, pages 331–339, 2019. 8
- [31] Olga Russakovsky, Jia Deng, Hao Su, Jonathan Krause, Sanjeev Satheesh, Sean Ma, Zhiheng Huang, Andrej Karpathy, Aditya Khosla, Michael S. Bernstein, Alexander C. Berg, and Fei-Fei Li. ImageNet large scale visual recognition challenge. *International Journal of Computer Vision (IJCV)*, 115(3):211–252, 2015. 5
- [32] Andrei A Rusu, Dushyant Rao, Jakub Sygnowski, Oriol Vinyals, Razvan Pascanu, Simon Osindero, and Raia Hadsell. Meta-learning with latent embedding optimization. In *ICLR*, 2019. 3
- [33] Victor Garcia Satorras and Joan Bruna. Few-shot learning with graph neural networks. In *ICLR*, 2018. 2, 3, 5, 6, 7, 8, 9
- [34] Michael Schlichtkrull, Thomas N Kipf, Peter Bloem, Rianne Van Den Berg, Ivan Titov, and Max Welling. Modeling relational data with graph convolutional networks. In *European Semantic Web Conference*, pages 593–607, 2018. 3
- [35] Edgar Schonfeld, Sayna Ebrahimi, Samarth Sinha, Trevor Darrell, and Zeynep Akata. Generalized zero- and few-shot learning via aligned variational autoencoders. In *CVPR*, pages 8247–8255, 2019. 3
- [36] Eli Schwartz, Leonid Karlinsky, Joseph Shtok, Sivan Harary, Mattias Marder, Abhishek Kumar, Rogério Feris, Raja Giryes, and Alex Bronstein. Delta-encoder: an effective sample synthesis method for few-shot object recognition. In *Advances in Neural Information Processing Systems*, pages 2850–2860, 2018. 3
- [37] Lei Shi, Yifan Zhang, Jian Cheng, and Hanqing Lu. Two-stream adaptive graph convolutional networks for skeleton-based action recognition. In *CVPR*, pages 12026–12035, 2019. 3
- [38] Martin Simonovsky and Nikos Komodakis. Dynamic edge-conditioned filters in convolutional neural networks on graphs. In *CVPR*, pages 3693–3702, 2017. 2, 3
- [39] Jake Snell, Kevin Swersky, and Richard Zemel. Prototypical networks for few-shot learning. In *Advances in Neural Information Processing Systems*, pages 4077–4087, 2017. 1, 3, 6, 7, 8
- [40] Flood Sung, Yongxin Yang, Li Zhang, Tao Xiang, Philip HS Torr, and Timothy M Hospedales. Learning to compare: Relation network for few-shot learning. In *CVPR*, pages 1199–1208, 2018. 1, 3, 8
- [41] Oriol Vinyals, Charles Blundell, Timothy Lillicrap, koray kavukcuoglu, and Daan Wierstra. Matching networks for one shot learning. In *Advances in Neural Information Processing Systems*, pages 3630–3638, 2016. 1, 3, 5, 6, 7, 8
- [42] Catherine Wah, Steve Branson, Peter Welinder, Pietro Perona, and Serge Belongie. The Caltech-UCSD birds-200-2011 dataset. Technical Report CNS-TR-2011-001, California Institute of Technology, 2011. 1, 5
- [43] Rex Ying, Ruining He, Kaifeng Chen, Pong Eksombatchai, William L Hamilton, and Jure Leskovec. Graph convolutional neural networks for web-scale recommender systems. In *KDD*, pages 974–983, 2018. 3
- [44] Jason Yosinski, Jeff Clune, Yoshua Bengio, and Hod Lipson. How transferable are features in deep neural networks? In *Advances in Neural Information Processing Systems*, pages 3320–3328, 2014. 1
- [45] Li Zhang, Xiangtai Li, Anurag Arnab, Kuiyuan Yang, Yunhai Tong, and Philip HS Torr. Dual graph convolutional network for semantic segmentation. *arXiv preprint arXiv:1909.06121*, 2019. 3

- [46] Long Zhao, Xi Peng, Yu Tian, Mubbasir Kapadia, and Dimitris N Metaxas. Semantic graph convolutional networks for 3D human pose regression. In *CVPR*, pages 3425–3435, 2019. 3
- [47] Ling Zhao, Yujiao Song, Chao Zhang, Yu Liu, Pu Wang, Tao Lin, Min Deng, and Haifeng Li. T-GCN: A temporal graph convolutional network for traffic prediction. *IEEE Transactions on Intelligent Transportation Systems*, 2019. 3
- [48] Dengyong Zhou, Olivier Bousquet, Thomas N Lal, Jason Weston, and Bernhard Schölkopf. Learning with local and global consistency. In *Advances in Neural Information Processing Systems*, pages 321–328, 2004. 6
- [49] Xiaojin Zhu, Zoubin Ghahramani, and John D Lafferty. Semi-supervised learning using Gaussian fields and harmonic functions. In *ICML*, pages 912–919, 2003. 6